POLITECNICO
MILANO 1863

SCUOLA DI INGEGNERIA INDUSTRIALE
E DELL'INFORMAZIONE

Simulation of Heat Transfer in Reciprocating Compressors

TESI DI LAUREA MAGISTRALE IN
ENERGY ENGINEERING
INGEGNERIA ENERGETICA

Author: **Alessandro Raneri**

Student ID: 10892919
Advisor: Antonio Giuffrida
Academic Year: 2024-25

Abstract

In this thesis, heat transfer in reciprocating-type compressors is modelled, which is of relevance due to its applicability to hydrogen gas storage. This is of great interest in facilitating the energy transition. This work contains and shows an overview of the technical literature, along with equations of the heat loss models proposed by a few scholars, namely Annand, Woschni, Adair, Disconzi, and Aigner. Detailed information on the implementation of these models in MATLAB, using the REFPROP library to obtain fluid properties, is presented. Later, preliminary results from the simulations are compared with the literature models, to assess the validity of the current model implementation, in a small reciprocating-piston compressor for refrigeration applications. The working fluids analysed are R134a, carbon dioxide, and dry air. A case study on a larger hydrogen reciprocating-piston compressor is then presented, with a parametric analysis performed on the wall temperature. It is ascertained that heat transfer in compressors requires consideration, although its effect is small compared to the power required for compression.

Key-words: reciprocating-piston compressors, heat loss models, hydrogen, heat transfer, compression.

Abstract in italiano

In questa tesi è stato modellato lo scambio termico nei compressori alternativi a pistoni, aspetto rilevante con riferimento alla possibile applicazione alla compressione dell'idrogeno. Una volta introdotto un esauriente riassunto della letteratura tecnica, unitamente alle equazioni e ai modelli di dispersione termica proposti da Annand, Woschni, Adair, Disconzi e Aigner, si è passati all'implementazione dei modelli in ambiente MATLAB, tenendo conto delle proprietà dei fluidi reali grazie a REFPROP. Quindi si sono confrontati i risultati delle simulazioni con risultati da letteratura, per valutare la validità dei modelli implementati, in un piccolo compressore alternativo a pistone per refrigerazione. I fluidi di lavoro analizzati sono R134a, anidride carbonica e aria secca. Successivamente, si dettaglia un caso studio per un compressore alternativo a pistone, di taglia più grande, per compressione di idrogeno, sviluppando anche un'analisi parametrica sulla temperatura della parete. In conclusione, sebbene lo scambio termico nei compressori alternativi è meritevole di attenzione, influisce limitatamente sulla potenza di compressione.

Parole chiave: compressori alternativi a pistone, modelli di dispersione termica, idrogeno, scambio termico, compressione.

Contents

Introduction

The issue of global warming requires a shift away from fossil fuels to renewable energy sources. However, solar and wind energy are intermittent, depending on weather and time of day. Hydrogen plays a key role in the energy transition, due to its flexibility for energy demand. As it is gaseous, its storage requires the use of compressors, to reduce the volume, thus facilitating its containment. Compressors are classified into two types: turbo compressors and volumetric compressors. In the former the fluid, which moves through the machine, is compressed by rotating vanes; in the latter the stationary fluid is compressed by moving parts. Volumetric compressors are better suited to hydrogen compression as they achieve greater pressures, thus lower volumes of the gas. These can be further classified as either reciprocating or rotary compressors. Reciprocating compressors may be used, which employ a piston, driven by a crank shaft, to compress the gas, thus achieving a higher pressure. The piston moves through a cylinder, which contains the gas. At the cylinder head there are suction and discharge valves, through which gas enters and leaves the compressor, respectively [1]. Compressed gas leaves the compressor, followed by the movement of the piston back to its initial position, for more fluid to enter the machine to be compressed in a new cycle.

Compression of gas leads to increases in temperature and pressure. Heat is transferred between the gas and the cylinder walls of the compressor itself, as the gas temperature varies with the volume it occupies. The ideal compressor cycle is an approximation neglecting valve losses, as well as heat transfer between the gas and the cylinder. This implies adiabatic walls of the compressor, thus at constant temperature. On the other hand, the real cycle includes valve losses and heat transfer. It accounts for the variation in temperature caused by changes in volume of the gas, as it is expanded or compressed by the piston's movement [1].

Although an adiabatic wall temperature may be a reasonable assumption for large compressors, for small compressors with high pressure ratios compression of the gas leads to high temperatures. As a result, the adiabatic assumption does not hold, and heat flux must be considered [2]. The compression generates heat, which must be accounted for due to its effect on compressor efficiency, as well as thermal stress placed on the components in the compressor. Modelling and simulating the compressor therefore requires models for heat loss of the gas, towards the compressor and ambient.

Reciprocating Compressor Operation

Reciprocating compressors are positive displacement machines, increasing internal fluid pressures by reducing the volume. The linear piston movement inside the reciprocating compressor is driven by the rotary movement of a crankshaft. During compression the piston moves from bottom- to top-dead centre, the distance between the two being the stroke length. At top-dead centre the volume of gas is at its minimum, the space it occupies is referred to as clearance. The working fluid rises in temperature, leading to heat transfer from the hotter fluid to the cooler compressor walls. During discharge fluid leaves the compressor through the discharge valve, when the piston is at top-dead centre. The expansion stage involves piston movement away from its top position, thus cooling the fluid. Suction involves inflow of 'fresh' working fluid into the compressor head, which is at a cooler temperature, this occurs when the piston is at bottom-dead centre, thus when the gas volume is at its maximum. Heat transfer during this step is in the opposite direction of that during the compression, as wall temperature is greater than that of the fluid [1] [3] [4].

As the piston moves towards its top position, during the compression phase, it generates a pressure wave which seals the suction valve; the discharge valve is also closed thus there is no in- or out-flow of gas. For the ideal cycle the compression phase is isentropic. Once discharge pressure is reached this valve opens, allowing a mass flow out of the compressor. This phase is isobaric for the ideal case. As the piston moves away from the top position an expansion wave is produced, closing the discharge valve. The suction valve is closed since gas pressure exceeds suction pressure, the expansion phase. Again, gas remains enclosed in the cylinder, and isentropic. The isobaric suction phase occurs once pressure drops to suction pressure and the valve opens, thus mass flows into the compressor. The work done by the piston on the gas over a cycle is the area under the pressure-Volume diagram (pV) curve, Figure 0.1a. In the Figure, "PMS" refers to the top position, "PMI" to the bottom position of the piston. Suction and discharge valves are labelled A and M respectively. V_m refers to clearance volume, whilst V_c refers to the volume of the cylinder. On the pV-diagram sections 1 to 2 represent compression, where a higher pressure is attained, at a lower volume. 2 to 3 is discharge, with a decrease in the volume which is isobaric in the ideal case. 3 to 4 is expansion, thus an increase in volume and decrease in pressure. 4 to 1 is suction, with an increase in volume at constant pressure [1].

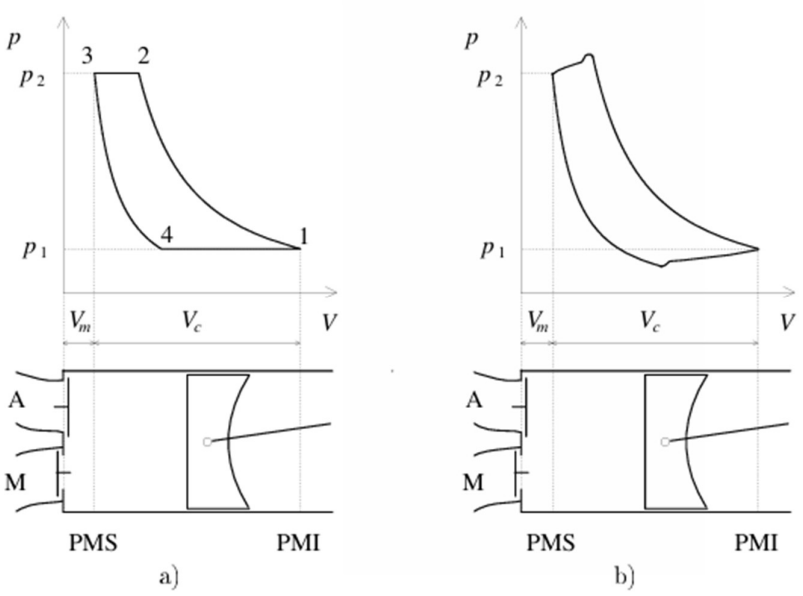

(a) Ideal Cycle (b) Real Cycle

Figure 0.1: pV-Diagrams of the Compressor Cycle, with corresponding Piston Position [1]

In the real cycle case, pressure losses of the gas flowing through the valves lead to the differences as seen in Figure 0.1b; during suction a pressure lower than suction pressure is reached, during discharge a pressure higher than discharge pressure is reached, caused by the opening and closing of the valves. Discharge and suction are therefore not isobaric. During compression and expansion phases the isentropic assumption does not hold due to the effect of wall temperature. During compression, once gas temperature exceeds that of the wall, the gas undergoes cooling due to heat transfer from gas to wall, although the gas temperature continues to rise due to compression. Likewise, during expansion, once gas temperature drops below that of the wall, the gas undergoes heating due to heat transfer from wall to gas, although temperature still diminishes due to expansion. Losses due to leakages may be neglected in the real case for a well-functioning machine [1].

State of the Art

The state of the art regarding the modelling of reciprocating compressors employs a three-dimensional analysis, however, due to long computational time it is more practical to adopt a quasi-one-dimensional approach. The piston of the compressor oscillates axially from bottom to top position, with equations of motion integrated over cylinder cross-section [5].

The modelling of heat transfer between fluid and compressor wall is in a developmental state [6], thus various heat transfer models require analysis and comparison amongst them. The state-of-the-art heat transfer models are referred to as “third generation”, which account for variations in fluid velocity, and are appropriate

for reciprocating compressors, as opposed to internal combustion engines. Mean piston velocity alone, which represents the axial direction, is insufficient to characterise the effects of fluid motion [6]. Radial direction may be accounted for using swirl velocity. Velocity through suction and discharge valves is also included in the state-of-the-art models. The models of Adair, Disconzi and Aigner may thus be termed as "third generation". These provide an advancement on "first- "and "second-"generation models.

Heat Transfer Modelling

The literature providing correlations for the heat loss model is vast, and results have been contradictory. Various approaches and equations have been used, without specific consensus on the most accurate model. This leads to the requirement of analysing and comparing various models, along with empirical data.

This thesis expands on previous work modelling an adiabatic hydrogen compressor, to include heat transfer from gas to cylinder wall. Case studies on both a small-scale and a large-scale compressor are performed. In the former case various working fluids and heat transfer models are analysed. Hydrogen gas as the working fluid is selected in the latter case, as well as an appropriate heat transfer model, the Disconzi model.

1 Literature Models about Heat Transfer in Reciprocating Compressors

The various heat transfer models from literature are compiled in this chapter, as well as those modelled in the thesis work.

1.1. History

In the last one hundred years, few correlations have been developed for heat transfer in cylinder-piston, reciprocating machines, due to difficulties in instantaneous measurements [7]. Early work on deriving correlations to accurately predict heat transfer were developed for Internal Combustion Engines (ICEs). The applicability of these for compressors may be unreliable, due to important differences between the two. Rotational speeds in ICEs are greater, and due to the combustion reaction the gas species involved will vary in composition, whereas in reciprocating compressors a single gas is used. Reciprocating compressors also employ piston movement, which affects gas velocity, thus correlations should account for this. However, models proposed by Annand and Woschni, although developed for ICEs, are commonly applied to reciprocating compressors, providing accurate results according to certain literature [8] [9]. The first correlation was developed by Nusselt, in 1923, for ICEs, and in 1928 for piston-machines in general, although today is considered only relevant historically. His work was expanded upon by later authors. Eichelberg, in 1939, provided a correlation for ICEs deemed to underestimate the heat transfer coefficient and, according to Annand, be contradictory to later work. "First generation" heat transfer models include Nusselt and Eichelberg's work, with the drawback of being of dimensional form [6]. Elser provided a correlation for a cylinder without combustion, however with errors, according to Annand. Woschni's correlation for ICEs was developed in 1967, determined experimentally, and widely applied to other reciprocating machines [7]. The models of Annand and Woschni constitute "second generation" models of heat transfer, and are of dimensionless form, thus may be scaled according to machine dimensions. Although some authors consider the application of these as accurate, a state-of-the-art, "third-generation" model for reciprocating compressors is required, which account for more complex fluid flow features [6].

A 1972 paper by Adair et al. [10] on heat transfer to the cylinder wall in reciprocating compressors presents a model for heat transfer, with experimental validation,

departing from previous work from various authors, including Nusselt, Annand and Woschni. Some models of heat loss in compressors require the division of the compressor cycle into four steps: compression, discharge, expansion and suction. Correlations can thus account for piston movement during compression and expansion, as well as in- and outflow of gas during suction and discharge, respectively. Heat transfer fluctuates, as well as changes direction, over the cycle depending on the step. This leads to the requirement for correlations specifically designed for compressors. Parameters or equations used must vary for each step. A single heat transfer correlation cannot therefore be reliably applied to a compressor [11]. The model proposed by Adair accounts for the piston movement in compressors by using swirl velocities, which vary depending on crank angle. Thus, although a single Nusselt correlation is used, velocity correlations vary depending on the step, and the Adair model can thus be considered as appropriate for reciprocating machines. Reynolds number as a function of swirl velocity is also present in the work of LeFeuvre, 1969. This differs from the work of previous authors, who use mean piston speed [7].

A 1984 paper on refrigerating compressors by Liu and Zhou [12] determines a heat transfer correlation from experimental data, although application to the diaphragm compressor may be inaccurate, due to their neglecting of transient wall temperature [7]. The wall temperature is taken as the average value over one cycle. A single Nusselt correlation is proposed, as well as swirl velocity correlations, which differ from those derived by Adair. A 1994 paper by Fagotti et al. [8] reports the Annand correlation to provide more accurate results than both Liu and Zhou's model, as well as Adair's. Literature provides conflicting results on which heat transfer model is best for compressors. Furthermore, coefficients provided for the Annand model vary between papers, thus it is unclear which is suitable [6] [13] [14].

Two papers by Tuhovcak et al. (2015,2016) compare five models in a reciprocating compressor [13] [14]: Annand, Woschni, Adair, Disconzi and Aigner models. The first four models analysed determine Nusselt number as function of Reynold's and Prandtl numbers, whereas the Aigner model applies the Stanton number in determining the heat transfer coefficient. Findings from these papers determine similar results in the calculation of volumetric efficiency for Annand, Woschni and Aigner models. A 2022 paper by Liu et al. concludes that Annand, Woschni, and Hohenberg models provide comparable trends, although the Adair model differs [15]. Tuhovcak et al. determine the Annand model to overestimate heat flux during the discharge step, however the Woschni model provides consistent results with other models over all four steps. The Adair model may underestimate heat flux during discharge and expansion. On the other hand, the Aigner model provides consistent heat fluxes with the average of the five models evaluated, across all cycle steps. It applies Stanton number, which is directly proportional to friction coefficient, and correlations for the latter are provided for compression and expansion, and suction and discharge [13] [14]. It is this

variability of the Aigner model which may make it a suitable candidate for accurate heat transfer prediction. Furthermore, velocities used in determining the Reynold's number vary; for compression and expansion, mean piston speed is used, whereas for suction and discharge it is the velocity of flow through the valve. The Disconzi model also benefits from various correlations applied for each step. As in the case of the Aigner model it was developed specifically for reciprocating compressors and provides Nusselt correlations where coefficients change for each step, as well as velocity in the Reynold's equation. Piston velocity is used for compression and expansion, whereas during suction and discharge different correlations are employed, accounting for both piston velocity and flow through valves. Accounting for the latter is important as it greatly affects heat transfer. However, disadvantages of this model according to the authors include overestimation of both the heat flux during suction, and isentropic and volumetric efficiency. Furthermore, experimental validation is required as the Disconzi model is the result of a numerical study [7]. Thus, in determining efficiency Annand, Woschni and Aigner models may be optimal, whereas Adair and Disconzi models benefit from being derived for reciprocating compressors, which the Aigner model is. The papers may imply this model as potentially the best. However, Adair, Disconzi and Aigner models all comply with state-of-the-art requirements concerning calculation of the fluid velocity in reciprocating compressors, thus are likely better models than those of Annand and Woschni. In this thesis work these five aforementioned models are compared and applied to a reciprocating compressor, in Chapter 3. The model of Disconzi is selected for application to a hydrogen reciprocating compressor, in Chapter 4.

1.2. Heat Transfer Models

The heat transfer model selected, in most cases, determines the Nusselt number and therefore the heat transfer coefficient. These vary with time, over the cycle, and must be calculated for each timestep in MATLAB. Most models determine Nusselt number as a function of Reynold's and Prandtl, with coefficients varying between models as in Equation (1.1):

$$Nu = aRe^{b}Pr^{c} \tag{1.1}$$

$$Nu = \frac{hL_c}{k} \tag{1.2}$$

The characteristic length, L_c, in Equation (1.2) varies between models. The transient effect on fluid properties over the cycle must be considered, REFPROP is used to determine instantaneous values; due to variations in temperature and pressure, properties such as gas density, ρ_g, vary widely and may not be assumed constant [11]. Mass and volume of gas in the compressor head are represented by m_g and V_g, respectively, in Equation (1.3).

$$\rho_g(t) = \frac{m_g(t)}{V_g(t)} \tag{1.3}$$

According to Fagotti et al. and Fonseca et al., comparing time-averaged values for heat flux provides comparative results between models, although instantaneous values differ considerably [8] [9].

1.2.1. Annand model [14]

The Nusselt correlation for the Annand model varies between authors. The correlation applied in this work is presented in Equation (1.4), proposed by Tuhovcak et al. in their 2016 paper [14]:

$$Nu = 0.7Re^{0.7}Pr^{0.7} \tag{1.4}$$

Reynold's number employs mean piston speed, u_p, as in Equation (1.5). Gas viscosity is represented by μ_g, calculated using REFPROP. Cylinder diameter or "bore" is represented by D.

$$Re = \frac{\rho_g D u_p}{\mu_g} \tag{1.5}$$

1.2.2. Woschni model [14]

The Woschni model also has many variations between authors, the form of the Nusselt expression proposed by Tuhovcak is presented in Equation (1.6):

$$Nu = 0.035Re^{0.7} \tag{1.6}$$

$$Re = \frac{\rho_g D u}{\mu_g} \tag{1.7}$$

Velocity, u, in Equation (1.7) is calculated during discharge and suction steps, and during compression and expansion, with the following two expressions in Equation (1.8):

$$\begin{cases} u = 6.618u_p & discharge, suction \\ u = 2.28u_p & compression, expansion \end{cases} \tag{1.8}$$

1.2.3. Adair model [10]

The authors propose an experimentally validated model of heat transfer for a reciprocating refrigerating compressor, although they do not provide information on the fluid, nor dimensions of the compressor. An equivalent diameter D_e is used in the Adair model, whereas generally cylinder diameter D is taken as characteristic length. According to the Adair model [10] [14]:

$$Nu = 0.053 Re^{0.8} Pr^{0.6} \tag{1.9}$$

$$D_e = \frac{6 \cdot Cylinder\ Volume}{Cylinder\ Area} \tag{1.10}$$

$$Re = \frac{\rho_g D_e u}{\mu_g} \tag{1.11}$$

Equation (1.9) presents the Nusselt correlation, whereas the Reynolds expression is reported in Equation (1.11). The equivalent diameter is calculated as in Equation (1.10). It accounts for movement of the piston through the piston-to-cylinder lead distance, which is used to calculate both cylinder volume and area.

Gas velocity in the cylinder, u, is calculated in Equation (1.12) from the swirl velocity, ω_g, which approximates the angular speed of the crankshaft. This varies with crank angle, φ; where ω is rotational speed:

$$u = \frac{D_e}{2} \omega_g \tag{1.12}$$

$$\begin{cases} \omega_g = 2\omega[1.04 + cos(2\varphi)] & \frac{3}{2}\pi < \varphi < \frac{1}{2}\pi \\ \omega_g = \omega[1.04 + cos(2\varphi)] & \frac{1}{2}\pi < \varphi < \frac{3}{2}\pi \end{cases} \tag{1.13}$$

The Equation (1.13) is derived from work by Shipinski, who suggests that swirl velocity is approximately twice the angular velocity, and cited in Adair's paper [10]. Crank angle is measured from bottom-dead centre.

Valve opening occurs when pressure drop exceeds zero and are otherwise closed; it is assumed that suction and discharge valves are either fully open or closed. Open valves constitute suction and discharge phases of the compressor cycle, whereas closed valves pertain to compression and expansion [10].

1.2.4. Disconzi model [16]

The model proposed by the authors is derived from a numerical study on a small reciprocating, refrigerating compressor, with R134a rotating at 3000 rpm. Compressor dimensions are provided, as well as suction temperature and pressure, and wall temperature. Walls excluding that of the cylinder are treated as adiabatic [16].

Disconzi's model, for coefficients in the Nusselt Equation (1.1), are reported in Table 1.1:

Table 1.1: Coefficients in the Disconzi Model, according to the Phase of the Compressor Cycle

Step	**Coefficients**		
	a	b	c
Compression	0.08	0.8	0.6
Discharge	0.08	0.8	0.6
Expansion	0.12	0.8	0.6
Suction	0.08	0.9	0.6

During compression and expansion Reynolds number uses solely piston mean velocity as in Equation (1.14), where stroke length is c, and frequency in Hertz, f:

$$\begin{cases} Re = \dfrac{\rho_g D u_p}{\mu_g} \\ u_p = 2 \times c \times f \end{cases} \tag{1.14}$$

Reynolds expressions during discharge and suction phases, respectively Equations (1.15a) and (1.15b) involve both piston and gas velocities:

$$Re = \frac{\rho_g D\left[u_p + {u_p}^{0.8}{u_c}^{0.2}\right]}{\mu_g} \tag{1.15a}$$

$$Re = \frac{\rho_g D\left[u_p + 2{u_p}^{-0.4}{u_c}^{1.4}\right]}{\mu_g} \tag{1.15b}$$

Equation (1.16) calculates gas velocity u_c which is a function of mass flowrate through the valve, and A_c pertains to cylinder cross-sectional area:

$$u_c(t) = \frac{\left|\dot{m}_g(t)\right|}{\rho_g A_c} \tag{1.16}$$

1.2.5. Aigner model [5]

The authors' model is presented for a reciprocating compressor, the paper presents one- and two- dimensional models, which greatly reduce computational time, with respect to three-dimensional models. For two-valve barrel design compressors they deem a quasi-one-dimensional model appropriate. Fluid properties, pressures, and compressor dimensions are reported [5]. The Aigner model employs Stanton number rather than a Nusselt correlation of the form presented in Equation (1.17):

$$St = \frac{h}{\rho_g {c_p}_g u} = \frac{Nu}{RePr} = \frac{C_f}{2Pr^{2/3}} \tag{1.17}$$

Expressions to calculate the friction factor, C_f, are provided by Bejan, in Chapter 8 on turbulent duct flow [17], and used by Tuhovcak who references Bejan. They vary depending on the phase as in Equation (1.18):

$$\begin{cases} C_f = 0.078Re^{-0.25} & compression, expansion \\ C_f = 0.046Re^{-0.2} & suction, discharge \end{cases} \tag{1.18}$$

For the former case the velocity in the Reynold's expression is that of the piston, for the latter it is the flow through the suction or discharge valve, respectively Equations (1.14) and (1.19). The formula for compression and expansion is applicable for Reynold's numbers below 8×10^4, whereas for suction and discharge a formula for higher Reynold's is required, in the range of $2 \times 10^4 < Re < 10^6$. This is due to greater turbulence effects when the valves are open. Suction valve area is represented by A_{in}, whilst that of the discharge valve is A_{out}.

$$\begin{cases} u_{suction}(t) = \dfrac{|\dot{m}_{in}(t)|}{\rho_g A_{in}} \\ u_{discharge}(t) = \dfrac{|\dot{m}_{out}(t)|}{\rho_g A_{out}} \end{cases} \tag{1.19}$$

2 Heat Transfer Model Implementation in MATLAB

Initially, before implementing a model for a large-scale hydrogen compressor, small-scale compressor models were developed using various heat loss models. MATLAB files were compiled for each heat loss model, namely those of Adair, Disconzi, Aigner, Annand and Woschni.

The first section of code defines compressor geometry, rotational speed and operating pressures, as well as suction temperature. The fluid is defined. Equations for piston position and its derivative, the piston speed, are defined. Piston position varies sinusoidally, with crank angle θ, Equation (2.1):

$$x = r\left(1 - \cos\theta + \mu - \sqrt{\mu^2 - \sin\theta^2}\right) \tag{2.1}$$

Where r is the crankshaft radius, which is half of the stroke length, and μ is the ratio of the connecting rod length to r. The geometry of the compressor is presented in Figure 2.1.

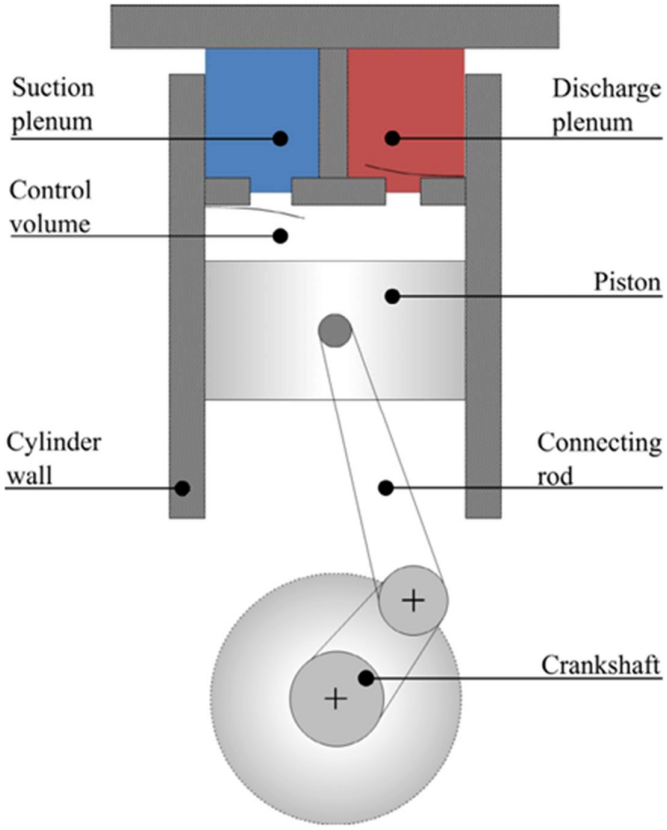

Figure 2.1: Reciprocating Compressor Geometry [14]

Equation (2.2) provides the piston speed:

$$xp = r\left(\sin\theta + \frac{0.5}{\sqrt{\mu^2 - \sin\theta^2}}\sin 2\theta\right) \tag{2.2}$$

The maximum cylinder volume is presented in Equation (2.3):

$$V_{max} = \frac{\pi}{4}D^2 c(1 + Clearance\ Ratio) \tag{2.3}$$

Ordinary Differential Equations (ODEs) are computed using MATLAB solvers such as ode113. The number of compressor cycles is defined, which when divided by the frequency gives the time, for the boundary condition in the ODE. REFPROP is used with suction temperature and pressure to determine density and specific internal energy of the fluid. Initial conditions in the ODE are mass and internal energy, the former being the product of the density and maximum cylinder volume, the latter being the product of the mass and the specific internal energy.

A number of compressor cycles are run with ode113 to reach a steady state, before a final cycle is run using Runge-Kutta's ode4 and plotted. This last cycle uses the final mass and internal energy of the previous cycles as initial conditions.

2.1. Thermodynamic Gas Model

The thermodynamic state is defined by Equations ((2.4a) and ((2.4b):

$$\begin{cases} \dfrac{\partial m_g}{\partial t} = \dot{m}_{g,in} - \dot{m}_{g,out} & \text{(2.4a)} \\ \dfrac{\partial U_g}{\partial t} = -hA\left(T_g - T_{wall}\right) + \left[\dot{m}_{g,in}h_{in} - \dot{m}_{g,out}h_{out}\right] - p_g\dfrac{\partial V_g}{\partial t} & \text{((2.4b)} \end{cases}$$

Where the former is mass variation over time due to suction and discharge, the latter is derived from the first law of thermodynamics for a non-adiabatic process. The first term on the right-hand side of the latter represents heat transfer from the gas to the cylinder wall. A positive heat rate occurs when gas temperature is below that of the wall, thus defined as positive entering the gas. The second term accounts for mass and enthalpy flows into and out of the system, and the third term accounts for volume variation of the gas. These equations are used in the function to solve the ODE.

Heat transfer coefficient, h, is dependent on the model selected, for which a vector of values is calculated using a "for" loop. Equations (2.5) and (2.6) provide the heat flux and heat rate, respectively, the latter being computed from instantaneous wall area, Equation (2.7):

$$q_{wall} = h\left(T_{wall} - T_g\right) \tag{2.5}$$

$$Q_{wall} = q_{wall}A \tag{2.6}$$

$$A = \pi D[c(1 + Clearance\ Ratio) - x] + 2\frac{\pi}{4}D^2 \tag{2.7}$$

Heat transfer over the final cycle, in Joules, is calculated using the "trapz" function from the heat rate and timestep. The power, in Watts, is the product of this and the frequency.

3 Results and Comparisons

The papers presented by Tuhovcak et al. [13] [14] are used to compare results for the heat transfer models implemented in MATLAB. Compressor dimensions are used as provided.

In the 2016 paper [14], the following compressor dimensions and boundary conditions are given, summarised in Table 3.1:

Table 3.1: Parameters of the Compressor in the Model

Parameter	**Value**	**Unit**
Cylinder bore	0.02	m
Stroke	0.02	m
Rod length	0.055	m
Crankshaft speed	3500	rpm
Clearance	0.07	mm
Suction pressure	1.15	bar
Discharge pressure	11.5	bar
Inlet temperature	50	°C
Wall temperature	90/140	°C

Analyses are performed varying rotational speed, wall temperature, and fluid species. Rotational speed is varied for three cases: 3500, 2950 and 2350 rpm. The fluids analysed in the paper are dry air, carbon dioxide, and refrigerants R134a and R404a. Total heat transfer and heat flux over a cycle are evaluated between different models of heat transfer: Annand, Woschni, Adair, Disconzi and Aigner models. Figure 3.1 a and b represent heat flux over a cycle for R134a and CO_2, respectively, where for the former the wall temperature is 90°C and for the latter 140°C. The dashed lines divide the cycle into compression, discharge, expansion and suction steps.

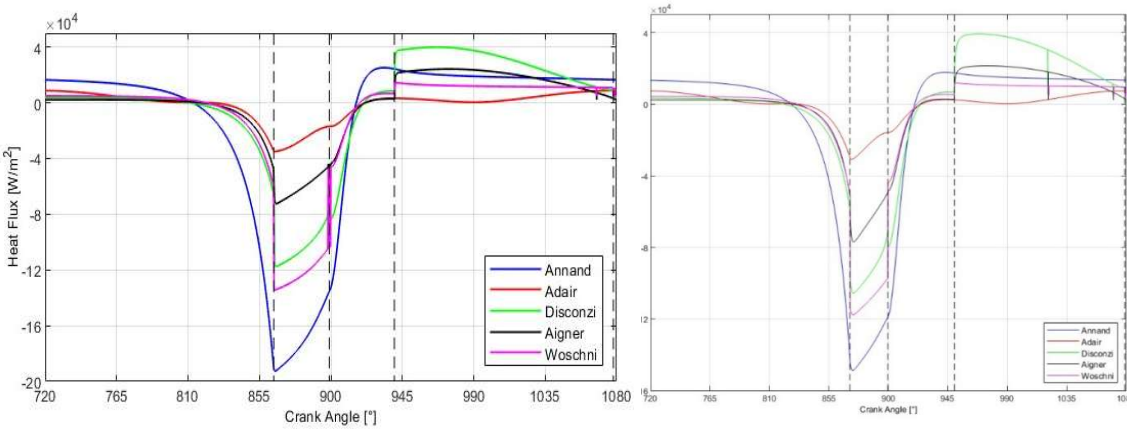

(a) Fluid R134a, with wall temperature of 90°C (b) Fluid CO_2, wall temperature 140°C

Figure 3.1: Heat Flux trends over a Cycle, according to the Crank Angle [14]

The minimum heat flux, in absolute values, is smallest for the Adair model, followed by Aigner, Disconzi, Woschni, with Annand having the greatest value. This order of size provides a guideline to follow in the models developed.

3.1. Adair Model

To compare results from the MATLAB code developed to the work by Tuhovcak, the fluids chosen are R134a, carbon dioxide and dry air. Table 3.2a presents results obtained with suction and wall temperatures held constant at 50°C and 90°C, respectively. Table 3.2b presents results for a wall temperature of 140°C, with suction temperature at 50°C. Rotational speed is varied as in the paper in the former table; in the latter it is constant at 3500rpm. Parameters are as follows: Q_{cycle} represents the thermal power, in Watts, and heat, in Joules, exchanged during the final cycle of the compressor. This latter value is provided by Tuhovcak's results for comparison. Q_{comp} represents compression power and work, in Watts and Joules respectively, over the final cycle. Minimum and maximum heat fluxes in the cycle are represented by q", and h_{max} represents maximum heat transfer coefficient in the cycle.

Table 3.2: Adair Model results for the Fluids

(a) Wall Temperature 90°C, varying Rotational Speed

Fluid	Parameter	Unit	3500rpm	2950rpm	2350rpm
R134a	Q_{cycle}	[W]	1,5412	1,5526	1,4904
		[J]	0,0264	0,0316	0,0381
	Q_{comp}	[W]	177,861	147,7831	114,7428
		[J]	3,049	3,0058	2,9296
	q"min	[W m^{-2}]	-2,30E+04	-1,90E+04	-1,40E+04
	q"max	[W m^{-2}]	6,30E+03	5,80E+03	5,10E+03
	hmax	[W m^{-2} K^{-1}]	431,778	375,632	308,274
CO2	Q_{cycle}	[W]	-1,3655	-1,0433	-0,7482
		[J]	-0,0234	-0,0212	-0,0191
	Q_{comp}	[W]	179,4731	147,9143	116,7014
		[J]	3,0767	3,0084	2,9796
	q"min	[W m^{-2}]	-3,00E+04	-2,50E+04	-2,00E+04
	q"max	[W m^{-2}]	3,20E+03	2,90E+03	2,60E+03
	hmax	[W m^{-2} K^{-1}]	179,098	153,846	126,756
Dry Air	Q_{cycle}	[W]	-2,0932	-1,7042	-1,3353
		[J]	-0,0359	-0,0347	-0,0341
	Q_{comp}	[W]	179,0636	149,1973	120,1005
		[J]	3,0697	3,0345	3,0664
	q"min	[W m^{-2}]	-3,20E+04	-2,70E+04	-2,20E+04
	q"max	[W m^{-2}]	2,80E+03	2,60E+03	2,30E+03
	hmax	[W m^{-2} K^{-1}]	115,539	100,241	82,8678

(b) Wall Temperature 140°C, at 3500rpm

Parameter	Unit	R134a	CO2	Dry Air
Q_{cycle}	[W]	7,8601	1,9953	0,6589
	[J]	0,1347	0,0342	0,0113
Q_{comp}	[W]	177,6112	180,0313	178,853
	[J]	3,0448	3,0863	3,0661
q"min	[W m^{-2}]	-3,00E+03	-2,30E+04	-2,70E+04
q"max	[W m^{-2}]	1,50E+04	8,00E+03	6,90E+03
hmax	[W m^{-2} K^{-1}]	432,679	178,057	114,427

As rotational speed is decreased, the heat exchange over one cycle increases, whilst compression power and work decrease. A slower cycle allows for more time for heat exchange between gas and wall to occur. Regarding compression power and work: as rotational speed decreases, so does the frequency, thus as the power required for compression is the product of the work required and the frequency, power decreases. The work required to compress the gas is provided in Equation (3.1):

$$Compression\ Work = -\oint p \times dV \tag{3.1}$$

As the differential of the volume is proportional to rotational speed, lowering the latter decreases work required. Heat transfer coefficient decreases with rotational speed as gas velocities are lower, leading to smaller values of Reynold's and Nusselt numbers. Comparing the fluids, the refrigerant R134a shows the greatest heat exchange and heat transfer coefficient.

The Table 3.3 summarises the results for heat exchange in Joules over the cycle, comparing the results from the paper. Rotational speed is at 3500rpm.

Table 3.3: Comparison of Total Heat Exchanged over a Cycle between the Adair Model and the Paper, with Percentage Variation

		Wall Temperature	
Fluid	**Parameter [J]**	**90°C**	**140°C**
R134a	Q_{cycle}	0,0264	0,1347
	$Q_{cycle,Tuhovcak}$	0,027	0,164
Error [%]		-2,3	-22
CO2	Q_{cycle}	-0,0234	0,0342
	$Q_{cycle,Tuhovcak}$	-0,041	0,026
Error [%]		-75	24
Dry Air	Q_{cycle}	-0,0359	0,0113
	$Q_{cycle,Tuhovcak}$	-0,061	-0,008
Error [%]		-70	170

Comparison of results between the paper and this work demonstrate similar results regarding heat exchange over a cycle, regarding the order of magnitude. Although some values differ significantly, such as in the case of air where wall temperature is set to 140°C, the differences in total heat transfer may be attributed to the shape of the heat flux graph, thus comparable order of magnitude is a better indication of accuracy rather than percentage of error. Furthermore, the paper provides insufficient detail on the models they constructed; thus, the results they provided should not be taken as sacrosanct.

Heat exchange over a cycle is calculated from the integral of the heat rate over time. As the heat rate is calculated from the difference between wall and gas temperature, a negative value of Q implies gas temperature is greater than wall temperature, which is to be expected as the gas is compressed thus reaching high temperatures. Heat transfer is thus in the direction of gas to wall. In the paper as well as in the code wall temperature is assumed, in two cases: at 90 and 140°C. During the compression cycle gas temperature must surpass wall temperature, otherwise the result would be meaningless: the temperature of the wall is due to the heat it receives from the gas. Therefore, it is expected that the value of total heat exchange over a cycle is negative. As wall temperature is assumed, the value is only appropriate if Q is negative, otherwise a lower wall temperature should be chosen. In the Adair model at 90°C both for Tuhovcak and for this project work, the values are negative for carbon dioxide and air, yet positive for the refrigerant. Thus, an assumption of wall temperature of 90°C is incorrect for the latter case. This leads to a requirement for a parametric analysis on wall temperature, presented in this work. Furthermore, the paper must be criticised for choice of wall temperature; instead of choosing a lower value, they then assume 140°C. This higher temperature is unreasonable for all fluids in the model, except for Tuhovcak's dry air model; all other values are positive.

The heat flux trend of the Adair model is presented in Figure 3.2 for the fluid R134a, at a rotational speed of 3500rpm and wall temperature 90°C. Highest heat fluxes occur during the suction phase, which have positive values as heat is transferred from the hotter walls to the cooler gas introduced. The compression phase is initially characterised by low yet positive values of heat flux, when the gas temperature is rising due to compression although still colder than the walls, then by increasingly negative values as gas temperature surpasses wall temperature, thus the direction of heat flow reverses. Once a minimum is reached at -23000 W m^{-2} the discharge phase begins and the hot gas leaves the compressor, until the reflex point on the curve, when the expansion phase starts. As the gas expands its temperature diminishes, initially it is still hotter than the walls, thus a negative yet increasing heat flux, until low positive values are reached: the gas cools due to expansion but it receives heat from the walls. The marked increase in the flux represents the suction phase, where fluid at suction temperature enters the compressor, to be compressed in a following cycle. The shape of the curve follows that reported by Tuhovcak, in Figure 3.1, with a maximum value, 6300 W m^{-2}, reached at the end of the cycle.

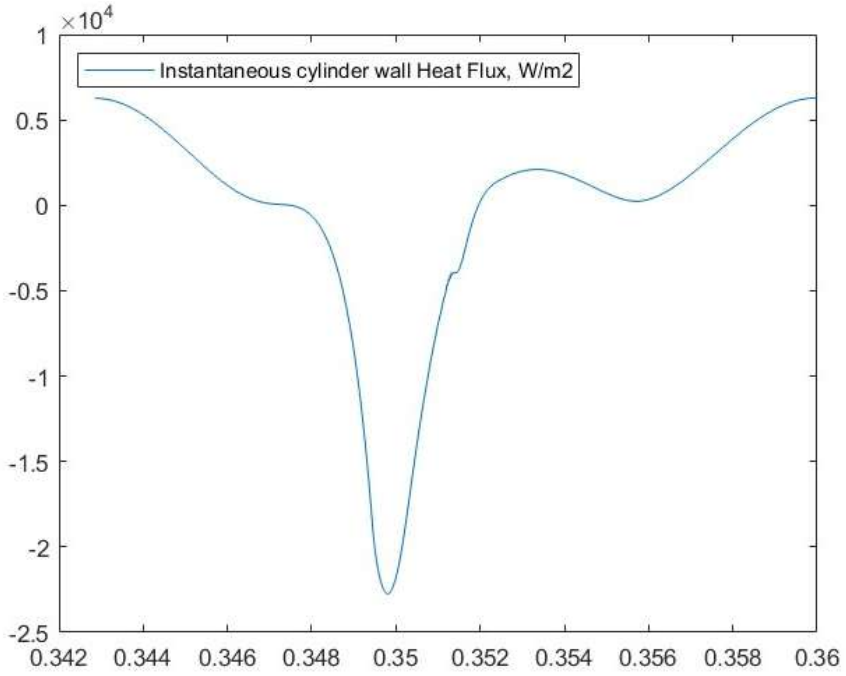

Figure 3.2: Heat Flux Trend of the Adair Model, for the Fluid R134a, at 3500rpm and Wall Temperature 90°C, as a function of Time

3.2. Disconzi Model

Table 3.4a presents results obtained with suction and wall temperatures held constant at 50°C and 90°C, respectively. Table 3.4b presents results for a wall temperature of 140°C.

Table 3.4: Disconzi Model results for the Fluids

(a) Wall Temperature 90°C, varying Rotational Speed

Fluid	Parameter	Unit	3500rpm	2950rpm	2350rpm
R134a	Q_{cycle}	[W]	9,4177	8,5408	7,1819
		[J]	0,1614	0,1737	0,1834
	Q_{comp}	[W]	110,3601	93,1262	73,4343
		[J]	1,8919	1,8941	1,8749
	q"min	[W m^{-2}]	-9,50E+04	-7,70E+04	-5,98E+04
	q"max	[W m^{-2}]	2,90E+04	2,70E+04	2,40E+04
	hmax	[W m^{-2} K^{-1}]	1545,78	1321,04	1076,32
CO2	Q_{cycle}	[W]	-3,888	-3,2068	-2,5218
		[J]	-0,0667	-0,0652	-0,0644
	Q_{comp}	[W]	127,8361	106,4149	83,5863
		[J]	2,1915	2,1644	2,1341
	q"min	[W m^{-2}]	-1,13E+05	-9,50E+04	-7,60E+04
	q"max	[W m^{-2}]	1,70E+04	1,50E+04	1,30E+04
	hmax	[W m^{-2} K^{-1}]	632,119	545,434	447,846
Dry Air	Q_{cycle}	[W]	-7,6621	-0,0606	-0,0608
		[J]	-0,1313	-2,9794	-2,3813
	Q_{comp}	[W]	139,4496	116,3661	92,085
		[J]	2,3906	2,3668	2,3511
	q"min	[W m^{-2}]	-1,17E+05	-3,70E+04	-3,00E+04
	q"max	[W m^{-2}]	1,80E+04	1,60E+04	1,30E+04
	hmax	[W m^{-2} K^{-1}]	428,966	142	120

(b) Wall Temperature 140°C, at 3500rpm

Parameter	Unit	R134a	CO2	Dry Air
Q_{cycle}	[W]	34,8301	7,6436	0,9294
	[J]	0,5971	0,131	0,0159
Q_{comp}	[W]	111,2892	127,5526	139,5904
	[J]	1,9078	2,1866	2,393
q"min	[W m^{-2}]	-4,60E+04	-9,50E+04	-1,08E+05
q"max	[W m^{-2}]	6,20E+04	3,50E+04	2,90E+04
hmax	[W m^{-2} K^{-1}]	1508,79	621,209	417,01

The assumption of wall temperature is inappropriate if the value of heat exchange over a cycle is positive, which is the case for the refrigerant at all three rotational speeds, with a wall temperature of 90°C. A wall temperature of 140°C is inappropriate for all three of the fluids examined.

The Table 3.5 summarises the results for heat exchange in Joules over the cycle, comparing the results from the paper, at 3500rpm.

Table 3.5: Comparison of Total Heat Exchanged over a Cycle between the Disconzi Model and the Paper, with Percentage Variation

		Wall Temperature	
Fluid	**Parameter [J]**	**90°C**	**140°C**
R134a	Q_{cycle}	0,1614	0,5971
	$Q_{cycle,Tuhovcak}$	0,137	0,52
Error [%]		15	13
CO2	Q_{cycle}	-0,0667	0,131
	$Q_{cycle,Tuhovcak}$	-0,076	0,101
Error [%]		-14	23
Dry Air	Q_{cycle}	-0,1313	0,0159
	$Q_{cycle,Tuhovcak}$	-0,246	-0,011
Error [%]		-87	169

The heat flux trend of the Disconzi model is presented in Figure 3.3 for the fluid R134a, at a rotational speed of 3500rpm and wall temperature 90°C. Compared to the Adair model, consistent with the paper, the Disconzi model reaches a greater minimum value of heat flux in absolute terms. The minimum in this case is -95000 W m^{-2}, compared to Adair's -23000 W m^{-2}. The shape of the curve also follows the results reported in the paper, with a comparatively large maximum reached, at 29000 W m^{-2}, prior to the end of the cycle. The maximum is greater than that of the Adair model.

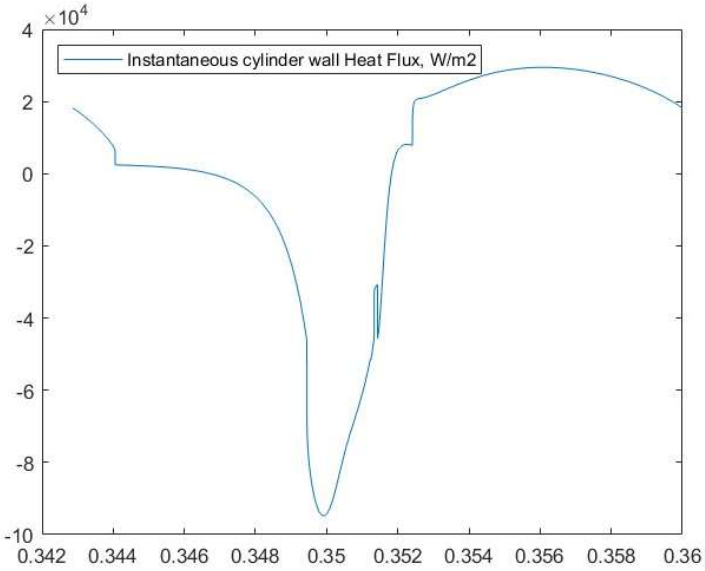

Figure 3.3: Heat Flux Trend of the Disconzi Model, for the Fluid R134a, at 3500rpm and Wall Temperature 90°C, as a function of Time

3.3. Aigner Model

The results are summarised in Table 3.6 a and b, for wall temperatures of 90 and 140°C, respectively.

Table 3.6: Aigner Model results for the Fluids

(a) Wall Temperature 90°C, varying Rotational Speed

Fluid	Parameter	Unit	3500rpm	2950rpm	2350rpm
R134a	Q_{cycle}	[W]	-4,264	-3,3415	-2,4194
		[J]	-0,0731	-0,068	-0,0618
	Q_{comp}	[W]	109,8448	92,9944	73,4758
		[J]	1,8831	1,8914	1,876
	q"min	[W m^{-2}]	-9,60E+04	-7,90E+04	-6,70E+04
	q"max	[W m^{-2}]	1,20E+04	1,04E+04	9,40E+03
	hmax	[W m^{-2} K^{-1}]	2849,96	2627,43	2410,96
CO2	Q_{cycle}	[W]	-8,582	-7,0839	-5,5257
		[J]	-0,1471	-0,1441	-0,1411
	Q_{comp}	[W]	128,8086	107,1878	84,1401
		[J]	2,2081	2,1801	2,1483
	q"min	[W m^{-2}]	-1,50E+05	-1,30E+05	-1,10E+05
	q"max	[W m^{-2}]	1,20E+04	1,10E+04	9,10E+03
	hmax	[W m^{-2} K^{-1}]	1416,66	1211,74	1001,96
Dry Air	Q_{cycle}	[W]	-9,8354	-8,2316	-6,4255
		[J]	-0,1686	-0,1674	-0,1641
	Q_{comp}	[W]	140,4205	117,0786	92,316
		[J]	2,4072	2,3813	2,357
	q"min	[W m^{-2}]	-1,70E+05	-1,50E+05	-1,10E+05
	q"max	[W m^{-2}]	1,40E+04	1,30E+04	9,70E+03
	hmax	[W m^{-2} K^{-1}]	871,035	874,114	607,024

(b) Wall Temperature 140°C, at 3500rpm

Parameter	Unit	R134a	CO2	Dry Air
Q_{cycle}	[W]	4,592	-4,3701	-6,7194
	[J]	0,0787	-0,0749	-0,1152
Q_{comp}	[W]	110,0948	128,9627	140,7313
	[J]	1,8873	2,2108	2,4125
q"min	[W m^{-2}]	-7,70E+03	-1,10E+05	-1,40E+05
q"max	[W m^{-2}]	1,90E+04	1,60E+04	1,80E+04
hmax	[W m^{-2} K^{-1}]	2900,82	1452,38	877,867

The assumption of wall temperature is inappropriate if the value of heat exchange over a cycle is positive. At 90°C all three fluids exhibit negative values, whereas at 140°C only R134a shows a positive value, thus for this fluid a lower wall temperature should be assumed instead.

Comparison with the paper is made in Table 3.7. Large differences in results are observed, especially at the higher wall temperature.

Table 3.7: Comparison of Total Heat Exchanged over a Cycle between the Aigner Model and the Paper, with Percentage Variation

		Wall Temperature	
Fluid	**Parameter [J]**	**90°C**	**140°C**
R134a	Q_{cycle}	-0,0731	0,0787
	$Q_{cycle,Tuhovcak}$	0,069	0,347
	Error [%]	194	-341
CO2	Q_{cycle}	-0,1471	-0,0749
	$Q_{cycle,Tuhovcak}$	-0,054	0,075
	Error [%]	63	200
Dry Air	Q_{cycle}	-0,1686	-0,1152
	$Q_{cycle,Tuhovcak}$	-0,084	0,017
	Error [%]	50	115

The heat flux trend of the Aigner model is presented in Figure 3.4 for the fluid R134a, at a rotational speed of 3500rpm and wall temperature 90°C. A minimum is reached of -96000 W m^{-2}. Contrary to the findings of Tuhovcak, this exceeds the minimum in the Disconzi model, -95000 W m^{-2}, although comparable in magnitude. The shape of the curve varies slightly in that following the minimum the curve does not immediately rise.

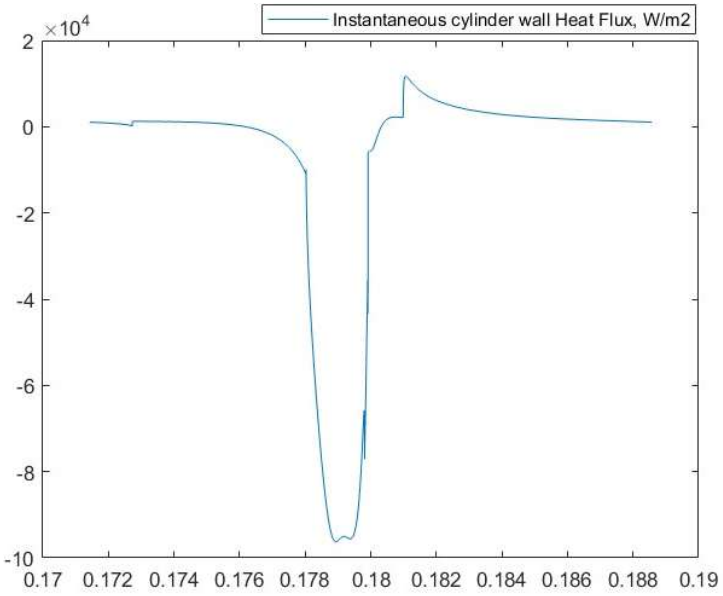

Figure 3.4: Heat Flux Trend of the Aigner Model, for the Fluid R134a, at 3500rpm and Wall Temperature 90°C, as a function of Time

3.4. Annand Model

The results are summarised in Table 3.8 a and b, for wall temperatures of 90 and 140°C, respectively.

Table 3.8: Annand Model results for the Fluids

(a) Wall Temperature 90°C, varying Rotational Speed

Fluid	Parameter	Unit	3500rpm	2950rpm	2350rpm
R134a	Q_{cycle}	[W]	-1,2019	-0,3356	0,3834
		[J]	-0,0206	-0,0068	0,0098
	Q_{comp}	[W]	110,3449	93,3937	73,7882
		[J]	1,8916	1,8995	1,884
	q"min	[W m^{-2}]	-1,33E+05	-1,10E+05	-8,70E+04
	q"max	[W m^{-2}]	2,10E+04	1,90E+04	1,70E+04
	hmax	[W m^{-2} K^{-1}]	2456,23	2126,92	1766,89
CO2	Q_{cycle}	[W]	-16,9258	-14,2773	-11,572
		[J]	-0,2902	-0,2904	-0,2955
	Q_{comp}	[W]	127,6091	106,1186	83,5064
		[J]	2,1876	2,1583	2,1321
	q"min	[W m^{-2}]	-1,84E+05	-1,57E+05	-1,31E+05
	q"max	[W m^{-2}]	2,50E+04	2,20E+04	2,00E+04
	hmax	[W m^{-2} K^{-1}]	1147,85	1011,91	861,7
Dry Air	Q_{cycle}	[W]	-23,5554	-20,2154	-16,6748
		[J]	-0,4038	-0,4112	-0,4257
	Q_{comp}	[W]	138,0248	115,2466	91,0882
		[J]	2,3661	2,344	2,3257
	q"min	[W m^{-2}]	-2,07E+05	-1,82E+05	-1,50E+05
	q"max	[W m^{-2}]	3,10E+04	2,80E+04	2,30E+04
	hmax	[W m^{-2} K^{-1}]	923,738	824,935	700,729

(b) Wall Temperature 140°C, at 3500rpm

Parameter	Unit	R134a	CO2	Dry Air
Q_{cycle}	[W]	24,5711	-3,654	-13,5176
	[J]	0,4212	-0,0626	-0,2317
Q_{comp}	[W]	112,2527	129,3315	140,496
	[J]	1,9243	2,2171	2,4085
q"min	[W m^{-2}]	-5,20E+04	-1,55E+05	-1,93E+05
q"max	[W m^{-2}]	2,70E+04	2,90E+04	3,40E+04
hmax	[W m^{-2} K^{-1}]	2420,97	1137,56	885,248

The assumption of wall temperature is inappropriate if the value of heat exchange over a cycle is positive. At 90°C all three fluids exhibit negative values, except R134a at a rotational speed of 2350rpm. Although the value for this fluid is negative at 2950rpm it is close to zero. For R134a if the assumption of wall temperature is appropriate at 3500rpm and considering that at lower rotational speed the assumption does not hold, an improvement would be to assume a wall temperature lower than 90°C at 2950rpm, and yet again a lower temperature for the case at 2350rpm. As rotational speed decreases so does the maximum temperature of the compressed fluid, thus leading to a lower wall temperature due to the reduction in heat transfer. The effect of lowering the rotational speed on heat transfer is apparent in Table 3.8a, with a decrease in heat transfer coefficient as well as heat flux. In Table 3.8b, at 140°C, only R134a shows a positive value, thus for this fluid a lower wall temperature should be assumed instead. The assumed wall temperatures provide meaningful results for both carbon dioxide and air, as values of total heat transferred during the cycle are negative in all cases.

Comparison with the paper is made in Table 3.9. Results are very close, except for the case of R134a at a wall temperature of 90°C. This may be due to an error in the author's model, due to a positive result which is close to zero.

Table 3.9: Comparison of Total Heat Exchanged over a Cycle between the Annand Model and the Paper, with Percentage Variation

		Wall Temperature	
Fluid	**Parameter [J]**	**90°C**	**140°C**
R134a	Q_{cycle}	-0,0206	0,4212
	$Q_{cycle,Tuhovcak}$	0,009	0,467
	Error [%]	144	-11
CO2	Q_{cycle}	-0,2902	-0,0626
	$Q_{cycle,Tuhovcak}$	-0,281	-0,057
	Error [%]	3,2	8,9
Dry Air	Q_{cycle}	-0,4038	-0,2317
	$Q_{cycle,Tuhovcak}$	-0,415	-0,247
	Error [%]	-2,8	-6,6

The heat flux trend of the Annand model is presented Figure 3.5 for the fluid R134a, at a rotational speed of 3500rpm and wall temperature 90°C. A large minimum is reached at -133000 W m^{-2}, which is expected both from Tuhovcak's results and due to the definition of the Nusselt equation, which features a large coefficient compared to other models.

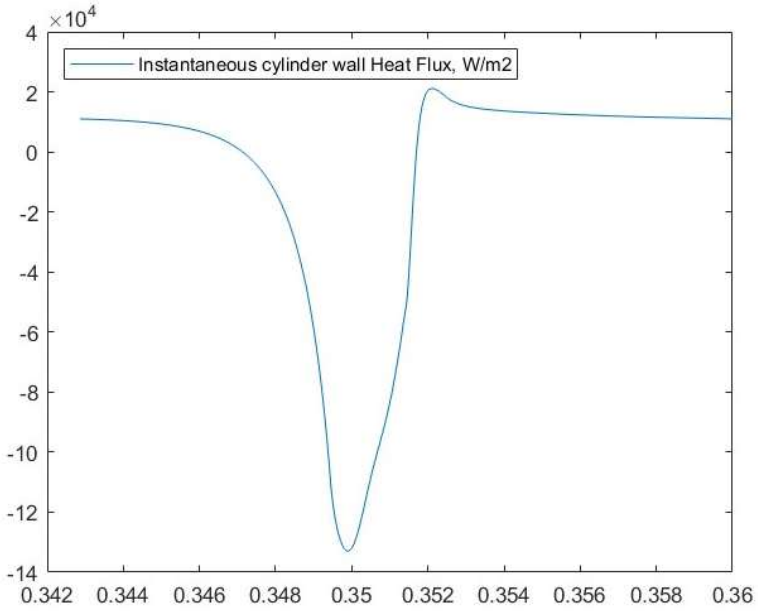

Figure 3.5: Heat Flux Trend of the Annand Model, for the Fluid R134a, at 3500rpm and Wall Temperature 90°C, as a function of Time

3.5. Woschni Model

The results are summarized in Table 3.10 a and b, for wall temperatures of 90 and 140°C, respectively.

Table 3.10: Woschni Model results for the Fluids

(a) Wall Temperature 90°C, varying Rotational Speed

Fluid	Parameter	Unit	3500rpm	2950rpm	2350rpm
R134a	Q_{cycle}	[W]	0,1881	0,303	0,3882
		[J]	0,0032	0,0062	0,0099
	Q_{comp}	[W]	109,967	93,0417	73,4988
		[J]	1,8851	1,8924	1,8766
	q"min	[W m^{-2}]	-2,80E+04	-2,30E+04	-1,80E+04
	q"max	[W m^{-2}]	3,50E+03	3,20E+03	2,80E+03
	hmax	[W m^{-2} K^{-1}]	546,244	473,699	393,813
CO2	Q_{cycle}	[W]	-3,5608	-2,9824	-2,3803
		[J]	-0,061	-0,0607	-0,0608
	Q_{comp}	[W]	128,7716	107,1534	84,1071
		[J]	2,2075	2,1794	2,1474
	q"min	[W m^{-2}]	-4,50E+04	-3,80E+04	-3,20E+04
	q"max	[W m^{-2}]	3,10E+03	3,00E+03	2,60E+03
	hmax	[W m^{-2} K^{-1}]	268,179	235,049	197,985
Dry Air	Q_{cycle}	[W]	-5,1731	-4,4227	-3,5946
		[J]	-0,0887	-0,09	-0,0918
	Q_{comp}	[W]	140,3657	117,154	92,3014
		[J]	2,4063	2,3828	2,3566
	q"min	[W m^{-2}]	-5,30E+04	-4,60E+04	-3,80E+04
	q"max	[W m^{-2}]	4,20E+03	3,80E+03	3,30E+03
	hmax	[W m^{-2} K^{-1}]	194,136	172,444	146,882

(b) Wall Temperature 140°C, at 3500rpm

Parameter	Unit	R134a	CO2	Dry Air
Q_{cycle}	[W]	6,1317	-0,1874	-2,2472
	[J]	0,1051	-0,0032	-0,0385
Q_{comp}	[W]	110,2893	128,9546	140,6711
	[J]	1,8907	2,2107	2,4115
q"min	[W m^{-2}]	-3,20E+03	-3,30E+04	-4,50E+04
q"max	[W m^{-2}]	7,10E+03	5,00E+03	6,00E+03
hmax	[W m^{-2} K^{-1}]	545,611	267,757	192,537

The assumption of wall temperature is inappropriate if the value of heat exchange over a cycle is positive, which is the case for the refrigerant at both wall temperatures. Although negative, the value of the heat exchange is close to zero for carbon dioxide in the case of wall temperature 140°C, thus a lower value should be assumed.

Comparison with the paper is made in Table 3.11. Results differ significantly, which may suggest an error in the Woschni model's implementation. In fact, in the 2015 paper by Tuhovcak et al., the Nusselt correlation of the Woschni model [13] is presented as in Equation (3.2), which differs from the expression reported in the 2016 paper, Equation (1.6). The coefficient differs by a factor of ten, which may indicate an erroneous usage of the Nusselt expression in the model.

$$Nu = 0.35Re^{0.7} \tag{3.2}$$

Table 3.11: Comparison of Total Heat Exchanged over a Cycle between the Woschni Model and the Paper, with Percentage Variation

		Wall Temperature	
Fluid	**Parameter [J]**	**90°C**	**140°C**
R134a	Q_{cycle}	0,0032	0,1051
	$Q_{cycle,Tuhovcak}$	-0,005	0,278
Error [%]		256	-165
CO2	Q_{cycle}	-0,061	-0,0032
	$Q_{cycle,Tuhovcak}$	-0,174	-0,036
Error [%]		-185	-1030
Dry Air	Q_{cycle}	-0,0887	-0,0385
	$Q_{cycle,Tuhovcak}$	-0,243	-0,133
Error [%]		-174	-245

The heat flux trend of the Woschni model is presented Figure 3.6 for the fluid R134a, at a rotational speed of 3500rpm and wall temperature 90°C. A minimum is reached at -28000 W m^{-2}, which is smaller than that reached in the paper at around -130000 W m^{-2}. Similarly to the large differences in results for heat exchange over the cycle, an error in implementation is probable. Furthermore, a maximum is reached at 3500 W m^{-2}, noticeable inferior to the author's result, at around 15000 W m^{-2}.

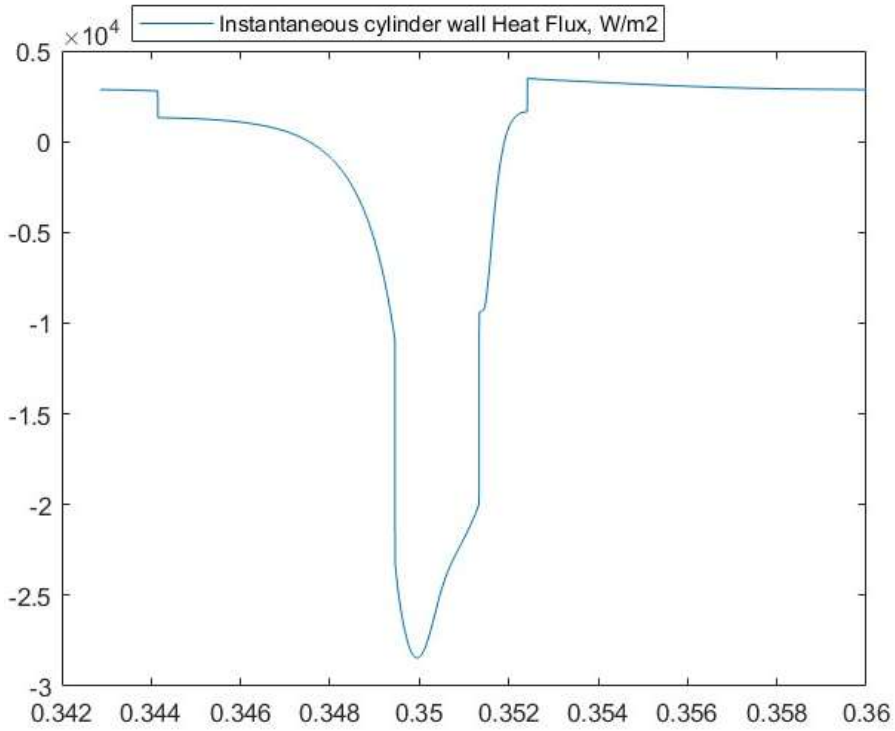

Figure 3.6: Heat Flux Trend of the Woschni Model, for the Fluid R134a, at 3500rpm and Wall Temperature 90°C, as a function of Time

3.6. Comparison between Models

The minima of the heat fluxes, achieved once compression reaches the discharge phase, must follow the following order according to the paper, increasing in absolute value: Adair, Aigner, Disconzi, Woschni, and Annand. Heat flux is proportional to the heat transfer coefficient, which increases with gas velocity. Velocity definitions vary between models, thus affecting heat flux values over the compressor cycle. Furthermore, correlations such as Nusselt and Reynolds, which have a direct bearing on the heat transfer coefficient, vary in formulation. The Annand model, demonstrating the greatest heat flux minimum, involves mean piston speed, as well as a coefficient of 0.7 in the Nusselt equation, Equation (1.4). Comparatively large heat flux values are thus expected, considering the smaller coefficients in Woschni and Adair models, 0.035 and 0.053, respectively. In changing this coefficient to 0.35 in Annand's model, heat flux was found to be much smaller, comparable to Adair and Disconzi. Woschni's model is expected to show large heat fluxes also, due to velocity being the mean piston speed multiplied by 6.618 or 2.28 depending on the phase, as shown in Equation (1.8). Disconzi's model involves comparable coefficients of 0.08 or 0.12 in the Nusselt expression, the coefficient 'a' in Table 1.1. Mean piston speed is used, although with Reynolds' expressions during discharge and suction being function of gas velocity, calculated using gas mass flowrate through the respective valve. In the Aigner model velocity is either that flowing through the valve or that of the piston, depending on the phase. Heat transfer coefficient is proportional to friction factor, whose low values are expected to contribute to lower heat fluxes. In developing the Aigner model an attempt was made using Haaland's equation for friction factor; larger values of the latter resulted in heat fluxes much greater than the other models, thus it was deemed appropriate instead to use the equations from Bejan, Equation (1.18). Adair's model shows the lowest heat flux, using velocity calculated from swirl velocity rather than that of the piston.

In agreement with the paper the lowest heat flux is achieved in the Adair model, quantitively -23000 W m^{-2}. However, Woschni follows at -28000 W m^{-2}, much lower than expected. Disconzi and Aigner follow, although results are of comparable magnitude, respectively -95000 W m^{-2}, and -96000 W m^{-2}. Annand shows the greatest value, -133000 W m^{-2}. The critical difference between findings lies in the Woschni model, which may be due to error in implementation.

Comparing total heat transfer over a cycle between models at 3500rpm, the models of Adair and Disconzi are similar in that the assumption of wall temperature of 90°C is inappropriate for R134a due to its positive value, although carbon dioxide and air show negative values. At 140°C all fluids exhibit positive values of total heat transfer, thus assuming this wall temperature when using Adair or Disconzi heat transfer models is incorrect. Aigner and Annand models are similar, 90°C may be an appropriate assumption for wall temperature for the three fluids, and at 140°C only

R134a shows a positive value. For the Woschni model at both wall temperatures R134a exhibits positive values; carbon dioxide and air both show negative values for each wall temperature case. Comparing results with the paper, Adair, Disconzi and Annand models are closest in findings for the total heat transfer. Across the models the order of magnitude of the total heat transfer is similar, in accordance with the literature [8] [9]. The model of Disconzi thus is deemed suitable for application in the following chapter, where a large-scale hydrogen compressor is analysed.

4 A Case Study for Hydrogen Compression

A case study applying the heat transfer model of Disconzi to a large-scale compressor is presented in this chapter. The working fluid is hydrogen gas, which is of interest due to its relevance and importance in the energy transition. A paper by Zhao et al. on hydrogen reciprocating compressors is used for compressor dimensions and operating conditions [18], presented in Table 4.1.

Table 4.1: Hydrogen Compressor Parameters

Parameter	**Value**	**Unit**
Cylinder bore	0.25	m
Stroke	0.18	m
Rod length	0.2	m
Crankshaft speed	300	rpm
Clearance volume	1.26E6	mm^3
Suction pressure	1	bar
Discharge pressure	2.5	bar
Inlet temperature	20	°C

Rotational speed is varied for three cases: at 300, 250 and 200rpm. A parametric analysis is performed on wall temperature. Thermal dispersion is calculated, which is expected to increase at lower rotational speeds due to greater heat exchange and lower gas velocity, u. It is calculated, as in Equation (4.1), from the heat exchange over a cycle in Watts and the average mass flowrate, which is taken as the average mass flowrate out of the system.

$$Disp = \frac{Q_{cycle}}{\dot{m}} \propto \frac{1}{u} \tag{4.1}$$

In varying the wall temperature, values of heat exchange over a cycle, as well as thermal dispersion, must be negative. This signifies heat transfer from hydrogen gas to the cylinder wall.

The behaviour of the system is analysed varying rotational speed and wall temperature. Due to a lack of results in the paper by Zhao et al. pertaining to the parameters investigated, a comparison is not made as in the previous chapter, instead results are analysed comparing the changes in behaviour.

4.1. Determining the Limit Wall Temperature

The value of the wall temperature for which thermal dispersion is equal to zero presents an upper limit. At this temperature, which varies according to the rotational speed, over a cycle the heat transfer conceded from the gas to the wall is equal to the heat received by the gas from the wall. Above this temperature, the value of thermal dispersion is positive and thus a meaningless solution; it implies wall temperature exceeding that of the gas. The limit temperature for each rotational speed is determined, thus during normal compressor operation the real wall temperature would be below this value. An initial investigation of the system's behaviour in varying the wall temperature is presented in Table 4.2:

Table 4.2: Effect of Wall Temperature on System Parameters, varying Rotational Speed

Wall Temperature [°C]	Parameter	Unit	300rpm	250rpm	200rpm
40	Q_{cycle}	[W]	-65,6569	-47,3875	-33,3924
		[J]	-13,1314	-11,373	-10,0177
	Q_{comp}	[W]	4470,5	3624,4	2824,1
		[J]	894,0927	869,8497	847,2244
	q"min	[W m^{-2}]	-1,00E+04	-8,50E+03	-6,80E+03
	q"max	[W m^{-2}]	7,10E+03	6,00E+03	4,90E+03
	hmax	[W m^{-2} K^{-1}]	337,814	295,97	248,555
	Disp.	[J/kg]	-21652	-18621	-16343
45	Q_{cycle}	[W]	20,0571	24,6678	25,3266
		[J]	4,0114	5,9203	7,598
	Q_{comp}	[W]	4466,4	3625,1	2825,2
		[J]	893,2845	870,0213	847,5587
	q"min	[W m^{-2}]	-1,00E+04	-8,20E+03	-6,60E+03
	q"max	[W m^{-2}]	8,10E+03	6,90E+03	5,70E+03
	hmax	[W m^{-2} K^{-1}]	336,963	295,136	247,808
	Disp.	[J/kg]	6650,4	9735,4	12453

Setting wall temperature to 40°C presents meaningful results; thermal dispersion values are negative for all three rotational speed cases. Orders of magnitude are $10^4 J/kg$. Conversely, at 45°C thermal dispersion is positive in all cases; thus, this wall temperature is beyond the limit in all cases. The heat loss changes sign, from negative in the former case, to positive in the latter. This leads to investigation of the wall temperature required to obtain a heat loss of zero, corresponding to the temperature limit of the wall. This limit wall temperature is the maximum possible temperature, and beyond this heat loss would be positive. For each rotational speed the limit wall temperature is computed; as rotational speed increases so does the limit temperature. The limits for each speed are presented in Table 4.3 where values of thermal dispersion are close to zero, with respect to the orders of magnitude observed in Table 4.2.

Table 4.3: Wall Temperature Limits for each Rotational Speed

Rotational Speed [rpm]	Wall Temperature Limit [°C]
300	43,8
250	43,28
200	42,85

4.2. Results

Further analyses are performed fixing wall temperature and varying rotational speed, and vice versa. The value of wall temperature is selected at 42.5°C, which is below the limit for each case. Rotational speed is varied as presented in Figure 4.1, and the curves of the heat flux over a cycle are plotted.

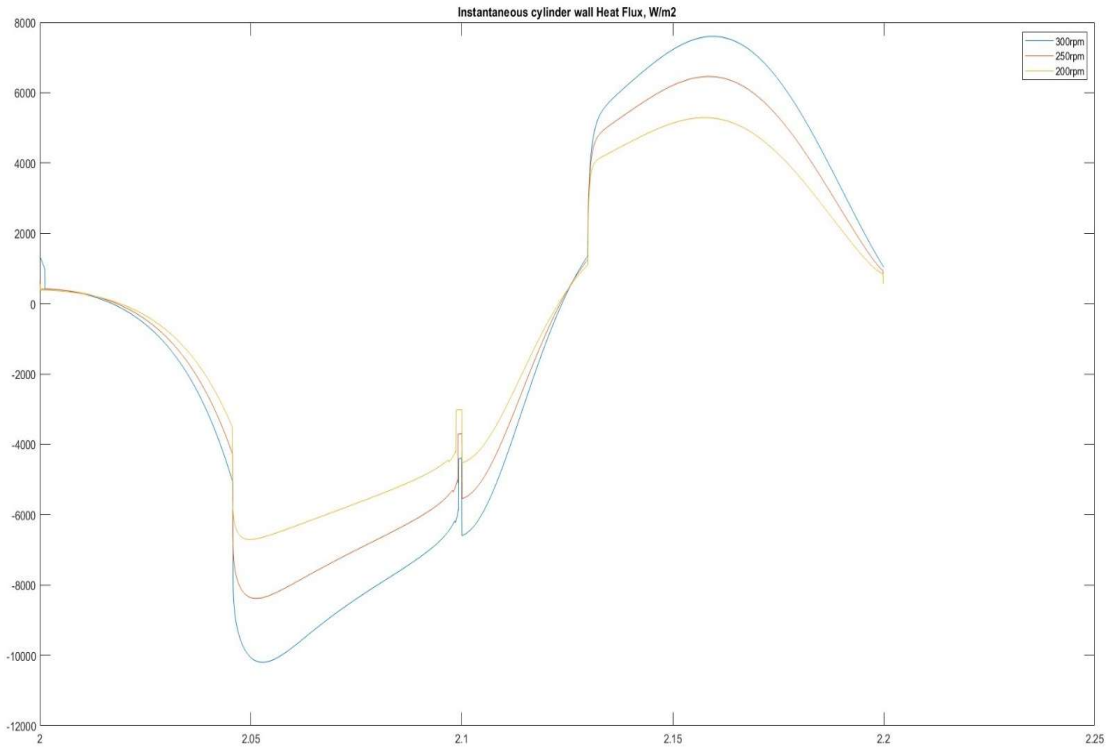

Figure 4.1: Heat Flux Trends varying Rotational Speed, at fixed Wall Temperature of 42.5°C

As rotational speed is reduced, the heat flux reduces in magnitude; both the maximum and minimum reduce in absolute value. A lower rotational speed leads to lower gas velocity and thus lower heat transfer coefficients, as seen in Equation (2.5) this leads to lower heat flux values. Gas temperatures reached are also lower, thus leading to a smaller temperature difference, as the wall temperature is fixed. This also contributes to lowering the absolute values of the heat flux.

Furthermore, rotational speed is fixed at 300rpm, and heat flux curves for three cases of wall temperature are plotted: 42.5, 40 and 37.5°C, as in Figure 4.2.

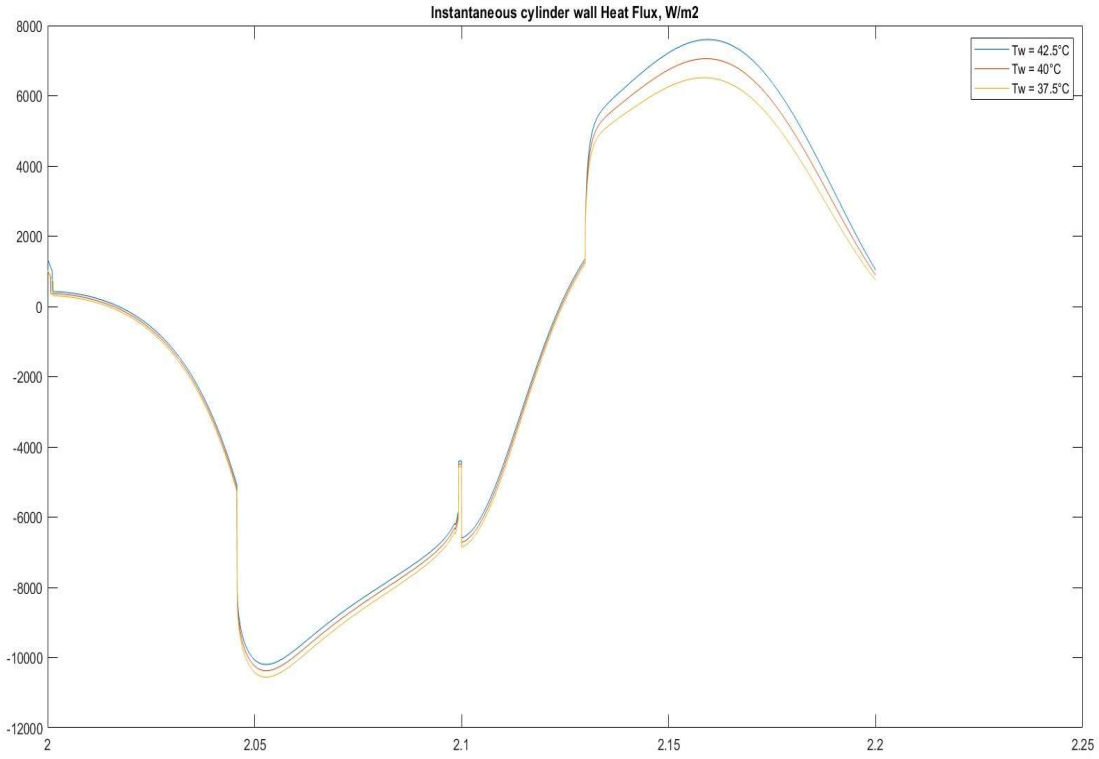

Figure 4.2: Heat Flux Trends varying Wall Temperature, at fixed Rotational Speed of 300rpm

As the wall temperature increases, the maxima of the heat flux increase, and the minima reduce in terms of absolute value. Higher wall temperature signifies greater heat transfer from the cylinder walls to the gas, thus where the curve of heat flux is positive these values will be greater, as heat transfer in this direction is denoted by the positive sign. This occurs primarily during expansion and suction phases. Where the curve is negative, values reduce in terms of absolute value, as the curve shifts toward the positive direction. Less heat is transferred from gas to wall, primarily during compression and discharge phases.

In fixing the wall temperature at 42.5°C and varying rotational speed, the effect of overpressure during discharge, and underpressure during suction is analysed. This is presented by means of a pV-Diagram, Figure 4.3, where the effects of over- and under-pressure are greater increasing the rotational speed. At a higher rotational speed a greater pressure is reached before the discharge valve opens. Likewise, a lower pressure is reached before the suction valve opens.

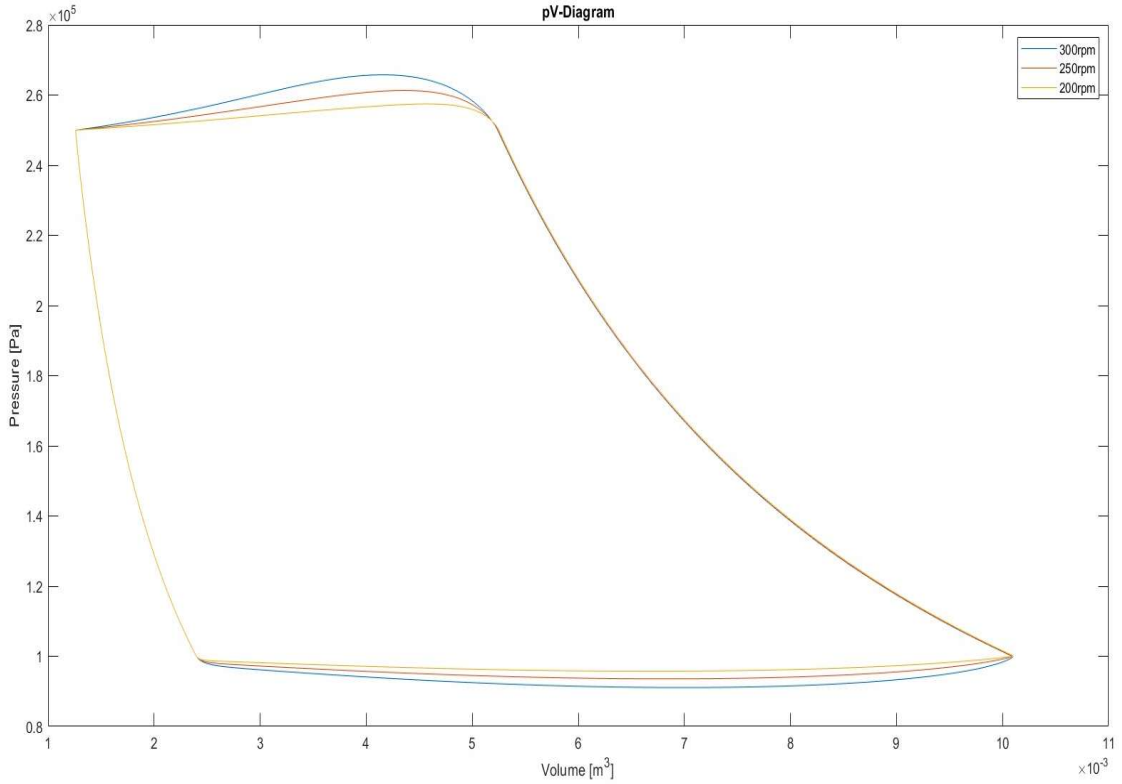

Figure 4.3: pV-Diagram varying Rotational Speed, at fixed Wall Temperature of 42.5°C

Comparison between the Disconzi model and the adiabatic case is made in Figure 4.4. At the start of the compression the curves coincide, thus the effect of heat transfer is negligible, although as the cycle progresses the heat loss model curve shifts to the left compared to the adiabatic case. This is due to the heat transfer from the gas to the wall, thus the cooling of the gas corresponds to a slightly lower volume. During discharge, the heat loss curve shows less overpressure due to the cooling of the gas, thus the pressures reached are slightly lower. As the expansion phase progresses, the heat loss curve shifts to the left; the mass of gas in the cylinder is less during this phase compared to the compression phase, where the curves are closer together. Expansion follows discharge, where gas exits the cylinder, leaving less gas in the machine. The effect of heat transfer is thus greater, leading to a visible discrepancy between the two curves. During suction the heat loss curve is slightly above that of the adiabatic case; the gas receives heat from the wall thus higher pressures are reached. In producing the figure, wall temperature is set to 42.5°C, with rotational speed of 300rpm.

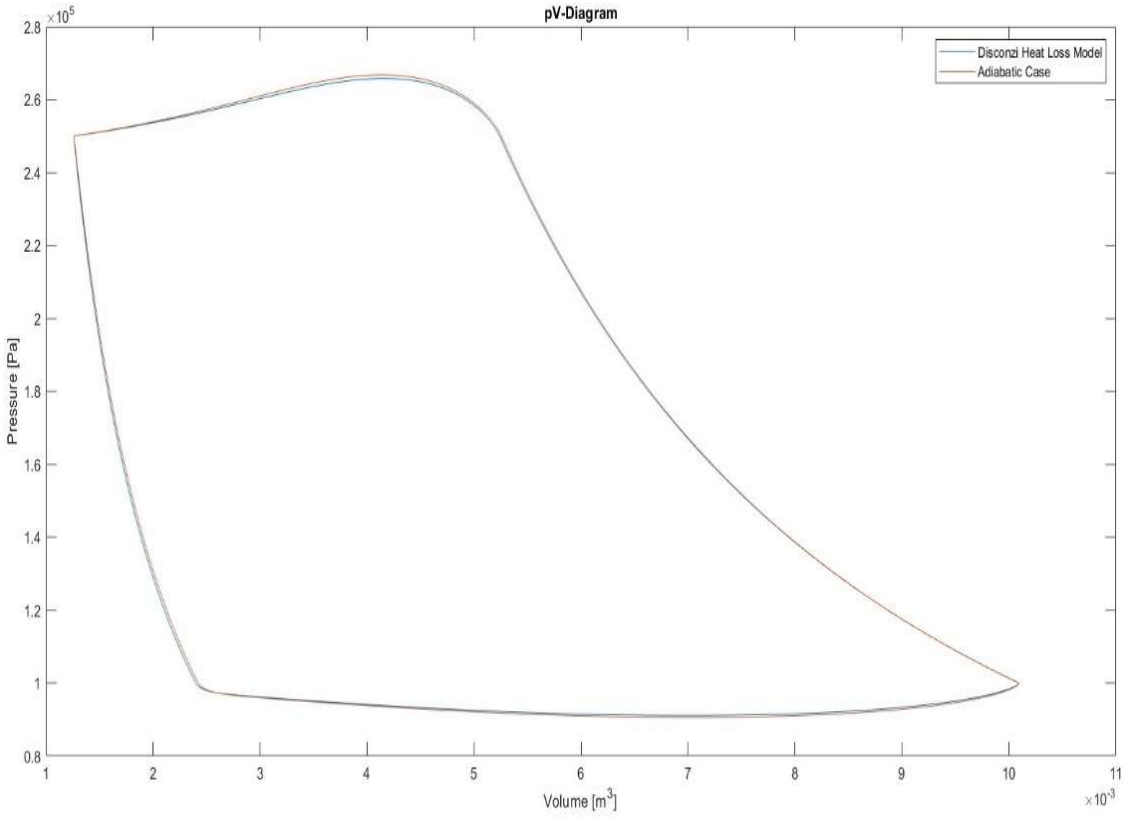

Figure 4.4: pV-Diagram comparing the Disconzi Heat Loss Model to the Adiabatic Case

The temperature-entropy diagram of the Disconzi model is presented in Figure 4.5, with wall temperature of 42.5°C and rotational speed of 300rpm. During the compression and discharge phases, entropy decreases due to heat transfer from gas to wall. Entropy increases slightly at the end of the expansion phase due to the wall heating the gas, which has reached a temperature below that of the wall.

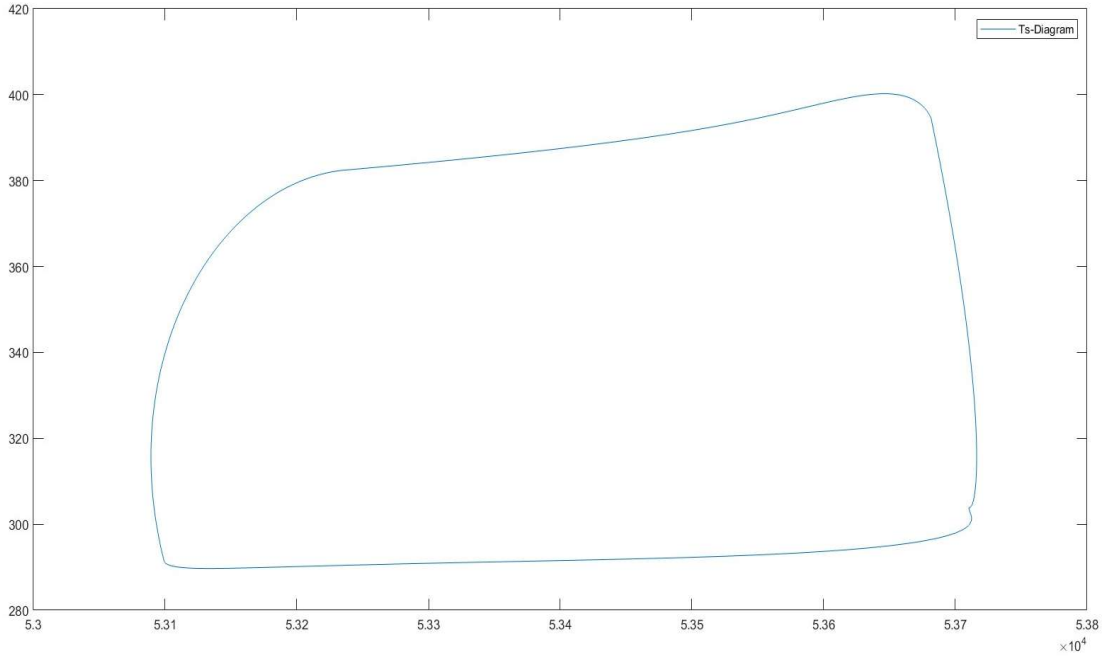

Figure 4.5: Ts-Diagram of the Hydrogen Compressor Cycle with the Disconzi model

5 Conclusion

In conclusion, heat loss models in reciprocating compressors were developed, starting from research into relevant literature. Five models were selected for implementation in MATLAB: Annand, Woschni, Adair, Disconzi, and Aigner. Numerical results were compared to a study by Tuhovcak et al. [14] to assess the validity of the developed models. In a small reciprocating compressor at 3500rpm, using the refrigerant R134a as working fluid, values of total heat transfer over a compressor cycle and the total compression power required were calculated. The percentage of the heat transfer with respect to the compression power for each model is as follows: 0.87% for Adair, 8.53% for Disconzi, -3.88% for Aigner, -1.09% for Annand, and 0.17% for Woschni. The effect of heat transfer between gas and wall within the compressor is thus small compared to the power required to compress the gas. A further case study was performed on a large-scale hydrogen compressor, using the Disconzi model, with compressor dimensions taken from a paper by Zhao et al. [18]. At a rotational speed of 300rpm with wall temperature set to 40°C, the percentage of heat transfer with respect to compression power is -1.47%. A parametric analysis was performed on wall temperature to determine the limits for three cases of rotational speeds.

An original selection of heat loss models was developed, and beyond possible implementation in hydrogen reciprocating-piston compressors, which are of interest in the energy transition, the models could be modified accordingly for usage in other types of reciprocating compressors. An example of a possible future development would be modifying the models for diaphragm compressors, which are also used in hydrogen compression and are thus of interest for global sustainability goals.

Bibliography

[1] L. A. Catalano and M. Napolitano, Elementi di Macchine Operatrici a Fluido, Bologna: Pitagora Editrice, 1998.

[2] T. Müllner, "Flow Patterns and Valve Dynamics in Multi-Valve Reciprocating Compressors," 2015.

[3] C. Willich and W. A. J, "Heat Transfer Losses in Reciprocating Compressors with Valve Actuation for Energy Storage Applications," *Journal of Energy Storage,* vol. 14, pp. 322-328, 2017.

[4] S. Kumar and G. S. L. R, "Heat Transfer Modeling and Simulation of Reciprocating Compressors - a Review," *JP Journal of Heat and Mass Transfer,* vol. 12, no. 1, pp. 31-44, 2015.

[5] R. Aigner and H. Steinrück, "Modelling Fluid Dynamics, Heat Transfer and Valve Dynamics in a Reciprocating Compressor," *5th Conference of the EFRC,* pp. 171-180, 2007.

[6] R. Keribar and T. Morel, "Heat Transfer and Component Temperature Prediction in Reciprocating Compressors," *International Compressor Engineering Conference,* vol. 658, pp. 454-463, 1988.

[7] B. Rutczyk and I. Szczygiei, "Development of Internal Heat Transfer Correlations for the Cylinders of Reciprocating Machines," *Energy,* vol. 230, 2021.

[8] F. Fagotti, M. L. Todescat, R. T. S. Ferreira and A. T. Prata, "Heat Transfer Modeling in a Reciprocating Compressor," *International Compressor Engineering Conference,* vol. 1043, pp. 605-610, 1994.

[9] L. Fonseca, R. Novella Rosa, P. Olmeda and V. RM, "Internal Combustion Engine Heat Transfer and Wall Temperature Modeling: An Overview," *Archives of Computational Methods in Engineering,* vol. 27, no. 5, pp. 1661-1679, 2019.

[10] R. P. Adair, E. B. Qvale and P. J. T, "Instantaneous Heat Transfer to the Cylinder Wall in Reciprocating Compressors," *International Compressor Engineering Conference,* vol. 86, pp. 521-526, 1972.

[11] W. H. Hsieh and W. T. T, "Experimental Investigation of Heat Transfer in a High-Pressure Reciprocating Gas Compressor," *Experimental Thermal and Fluid Science,* vol. 13, pp. 44-54, 1996.

[12] R. Liu and Z. Zhou, "Heat Transfer Between Gas and Cylinder Wall of Refrigerating Reciprocating Compressor," *International Compressor Engineering Conference,* vol. 441, pp. 110-115, 1984.

[13] J. Tuhovcak, J. Hejcik and J. M, "Modelling of Fluid Flow and Heat Transfer in a Reciprocating Compressor," *IOP Conference Series: Materials Science and Engineering,* vol. 90, 2015.

[14] J. Tuhovcak, J. Hejcik and J. M, "Comparison of Heat Transfer Models for Reciprocating Compressor," *Applied Thermal Engineering,* vol. 103, pp. 607-615, 2016.

[15] L. Z, Y. X, Y. X, Z. H and D. Z, "Performance Evaluation on the In-Cylinder Heat Transfer of a Reciprocating Compressor using CO2 as a Working Fluid," *Journal of Thermal Science,* vol. 31, no. 5, pp. 1518-1530, 2022.

[16] F. P. Disconzi, E. L. L. Pereira and C. J. Deschamps, "Development of an In-Cylinder Heat Transfer Correlation for Reciprocating Compressors," *International Compressor Engineering Conference,* 2012.

[17] A. Bejan, Convection Heat Transfer, Durham, North Carolina: John Wiley & Sons, Inc., 2013.

[18] D. Zhao, J. Zhang, Y. Wang, Y. Zhang, Z. Jiang and T. Dong, "Improvement of hydrogen reciprocating compressor efficiency: A novel capacity control system and its multi-objective optimization," *International Journal of Hydrogen Energy,* vol. 92, pp. 349-366, 2024.

List of Figures

List of Tables

List of symbols

Variable	Description	SI unit
A	instantaneous wall area	m^2
A_c	cylinder cross-sectional area	m^2
A_{in}	suction valve area	m^2
A_{out}	discharge valve area	m^2
c	stroke length	m
$c_{p,g}$	specific heat capacity at constant pressure of working fluid	$J\ kg^{-1}\ K^{-1}$
C_f	friction factor	-
D	cylinder diameter	m
D_e	equivalent diameter	m
$Disp.$	thermal dispersion	$J\ kg^{-1}$
f	frequency	Hz
h	heat transfer coefficient	$W\ m^{-2}\ K^{-1}$
h_{in}	enthalpy into system	$J\ kg^{-1}$
h_{max}	maximum heat transfer coefficient in a compressor cycle	$W\ m^{-2}\ K^{-1}$
h_{out}	enthalpy out of system	$J\ kg^{-1}$
k	thermal conductivity	$W\ m^{-1}\ K^{-1}$
L_c	characteristic length	m
m_g	mass of working fluid	kg
$\dot{m}_g$	mass flowrate through valve	$kg\ s^{-1}$
$\dot{m}_{in}$	mass flowrate through suction valve	$kg\ s^{-1}$
$\dot{m}_{out}$	mass flowrate through discharge valve	$kg\ s^{-1}$
Nu	Nusselt number	-
p_g	pressure of working fluid	Pa
Pr	Prandtl number	-
q_{wall}	heat flux	$W\ m^{-2}$
Q_{comp}	compression work	J
Q_{cycle}	heat exchange over a compressor cycle	J
Q_{wall}	heat rate	W

r	crankshaft radius	m
Re	Reynolds number	-
St	Stanton number	-
t	time	s
T_g	temperature of working fluid	K
T_{wall}	wall temperature	K
u	working fluid velocity	m s^{-1}
u_c	fluid velocity through valve	m s^{-1}
$u_{discharge}$	fluid velocity through discharge valve	m s^{-1}
u_p	mean piston velocity	m s^{-1}
$u_{suction}$	fluid velocity through suction valve	m s^{-1}
U_g	internal energy of working fluid	J
V_g	volume of working fluid	m^3
V_{max}	maximum cylinder volume	m^3
x	piston position	m
xp	piston speed	m s^{-1}
θ	crank angle	rad
μ	rod length divided by r	-
μ_g	dynamic viscosity of working fluid	Pa s
ρ_g	density of working fluid	kg m^{-3}
φ	crank angle	rad
ω	rotational speed	rad s^{-1}
ω_g	swirl velocity	rad s^{-1}

Acknowledgments

I would like to thank my advisor Antonio Giuffrida for his support in completing this thesis. Furthermore, I would like to thank the Politecnico di Milano for providing my master's degree education.